ACS OMEGA

Open Access

http://pubs.acs.org/journal/acsodf

Article

Optimization of Injection Source Settings for SNCR Numerical Simulation of Low-Water Content Biomass Boilers with Blending

Linmao Pu, Yu Gao,* Shengjun Zhong, Yong Zhang, Penglei Zhao, Lijuan Ji, Xinyu Liu, and Zhonghao Yan

Cite This: *ACS Omega* 2024, 9, 10207−10219

Read Online

ACCESS | Metrics & More | Article Recommendations

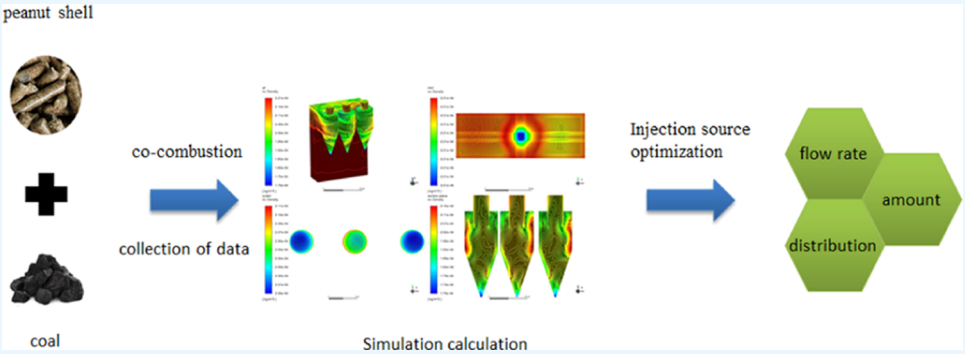

ABSTRACT: In order to control NO_x emissions and meet China's ultralow emission standards, a numerical simulation based on the computational fluid dynamics (CFD) approach is performed for the optimization of the reductant injection volume, number of injection sources, distribution, and injection direction for the flue gas denitrification process of a circulating fluidized bed boiler (CFB) blended with low-water content biomass in a 168 MW unit of a thermal power plant. Using the target power plant boiler entity as a template, a simplified geometric model is established, 1:1, and the mass fractions of each flue gas component set by the inlet boundary conditions are $O_2$2, H_2O11.6, $CO_2$16.2%, and NO0.05%(about 134 ppm), and the reduction reactions under different optimized conditions are numerically simulated using the SNCR model in ANSYS Fluent 2021 R1. The simulation results under each condition were analyzed. The results show that the optimal ammonia-to-nitrogen ratio should be taken as NSR = 1.25, the denitrification efficiencies of 81.00, 81.63, and 82.74% at the three outlets are high, and the ammonia escapes of 1.76, 2.08, and 9.42 mg/s are within a reasonable range; increasing the number of injection sources can significantly reduce the disturbance of the flue gas flow field by reductant injection; the direction of injection is parallel to the direction of the flue gas flow, and the line of the injection source is orthogonal to the direction of the flue gas flow, which is conducive to the mixing of the reductant and flue gas; the optimized boiler denitrification efficiency reaches 74.2%, meeting the ultralow emission requirements of nitrogen oxides and ammonia escape.

1. INTRODUCTION

Nitrogen oxides (NO_x), a large category of air pollution, include NO, NO_2, N_2O, N_2O_5, N_2O_3, NO_3, N_2O_4, etc. Approximately 70% of the Chinese annual NO_x emissions originate from the combustion of fossil fuels, with nearly half of these emissions occurring during the electricity generation process in coal-fired thermal power plants. NO is the primary NO_x constituent emitted from coal-fired boilers, followed by NO_2 accounting for about 5−10%, and the rest of the production is small enough to be negligible.[1,2] NO_x emissions from thermal power plants must be controlled due to their role in the formation of acid rain, contribution to photochemical smog, potential damage to the ozone layer, impact on atmospheric climate, and adverse effects on human health.[3] Inhalation of NO can lead to central nervous system damage, spasms, and acute poisoning, resulting in lung congestion, edema, and potentially fatal asphyxiation.[4]

All major power plants in China have adopted various NO_x control measures to meet the latest ultralow NO_x emission requirements (less than 50 mg/m^3). The stringency of NO_x emission standards, combined with their concentration in the postcombustion flue gas, dictates the choice of a specific control strategy among the various available denitrification methods.

Received: September 21, 2023
Revised: October 17, 2023
Accepted: October 19, 2023
Published: February 25, 2024

Table 1. Comparison of Post-treatment Methods for Nitrogen Oxides

method	process and applicability	reactant	product	advantages	disadvantages	max removal efficiency (%)	cost	refs
SCR	the NO_x is reduced to N_2 over the surface of catalysts at low temperatures (200−450 °C). applicability: large amounts of continuous flue gas.	NH_3, C_xH_y, CO, H_2, etc.	N_2	less secondary pollution, high removal efficiency, and mature technology.	catalysts are easily deactivated, ammonia leaks, and equipment is prone to corrosion.	80−95	relatively high	5−7
SNCR	reduction of NO_x to N_2 at high temperatures (800−1100 °C) without a catalyst. applicability: large amounts of continuous flue gas.	ammonia or urea.	N_2	no catalyst, low equipment, and operating costs, mature technology.	large amounts of NH_3, secondary pollution, and difficult to ensure the reaction temperature and residence time.	70−95	relatively low	8,9
alkali absorption	NO_x is oxidized as it passes through the alkaline solution and is then absorbed to form nitrate. applicability: small amounts of flue gas.	NaOH, $Ca(OH)_2$, NH_4OH, etc.	nitrate	the reproducibility of the adsorbent, the simplicity of the process equipment, the low investment, the significant effect, and some methods can recover NO_x.	low efficiency, high consumption of adsorbent, large space occupation, byproducts are not easy to handle, and low working temperature is not suitable for the treatment of boiler power plant flue gas.	10−50	relatively low	10−14
electron beam irradiation	NO_x reacts with fast electrons (300−800 keV) generated under electron beam irradiation to form nitric acid and a wide range of adaptability.		nitrate	less space occupation, simple operation, less secondary pollution, and simultaneous desulfurization and denitrification.	high energy consumption, radiation generation, and high technical content of key equipment, not easy to master.	70−90	high	15−19
catalytic oxidation absorption	NO_x is oxidized to nitrate when it passes through a solution containing an oxidizer in the presence of a catalyst. applicability: small amounts of flue gas.	H_2O_2, $KMnO_4$, $NaClO_2$, etc.	nitrate	high utilization rate of oxidizer, fast oxidation speed, high removal efficiency, simultaneous desulfurization and denitrification, recovery of NO_x and SO_2.	frequent catalyst poisonings, the temperature window is narrow and the equipment is huge.	70−95	high	3,7,20−23
complex absorption	NO_x is absorbed by the metal complex solution and rapidly forms metal-nitroso complexes. applicability: small amounts of flue gas.	Fe^{2+}-EDTA, $Co(NH3)_6^{2+}$, etc.	nitrate	mild reaction conditions, simple operation, low space occupation.	low filtration, difficult recovery of chelates.	10−60	high	24−26
bioprocesses	NO_x in flue gas is converted to organic nitrogen compounds or N_2 by the action of microorganisms. A wide range of adaptability.	microorganisms (denitrifying fungi, nitrifying archaea, etc.)	NO^{3-}/ NO^{2-} or N_2	less secondary pollution, low energy consumption, and simple process equipment.	the microbial environmental conditions are difficult to control, the removal efficiency is unstable, and the microbial life is short.	40−90	low	27−29

https://doi.org/10.1021/acsomega.3c07288
ACS Omega 2024, 9, 10207−10219

These control strategies depend on the combustion technology, fuel characteristics, whether the plant has been existing or is new, and applicable emission standards. A variety of methods are used to control stationary source emissions, from precombustion fuel cleaning to postcombustion off-gas treatment. Precombustion treatment involves seeking to reduce the nitrogen content of the fuel before it enters the combustion chamber, and fuel pretreatment is costly. The basic idea of in-combustion treatment is to create low-oxygen ambient conditions (especially in the early stages of combustion), reduce the flame temperature, or alter the residence time in various parts of the combustion zone to reduce NO_x formation and increase the inverse conversion of NO_x to N_2 and O_2. In-combustion treatments include low-excess air firing (LEAF), flue gas recirculation (FGR), and reburning (RB). Postcombustion treatment can be used as an alternative or supplement to combustion nitrogen control strategies, which involves the absorption or conversion of nitrogen oxides present in the postcombustion gas. Currently, the most common is selective catalytic reduction (SCR) and selective uncatalytic reduction (SNCR), in addition to alkali absorption, electron beam radiation, adsorption catalytic oxidation, complex absorption, microbial method, and other technologies (Table 1).

Due to the large volume of waste gas in thermal power plants, alkaline absorption and adsorption catalytic oxidation cannot be used; complex absorption usually needs to be combined with microbiological methods to remove byproducts, and microbiological methods and electron beam methods are difficult to achieve with automated control due to the complexity of equipment manipulation and are not used in thermal power plants; in contrast, SCR and SNCR are more suitable for flue gas denitrification treatment in thermal power plants, and both have their advantages and disadvantages, so combining them not only reduces the cost but also improves the efficiency; combining biomass blending with post-treatment SNCR to control boiler NO_x emissions is also a current research hotspot, which not only realizes the reuse of waste but also achieves the purpose of flue gas emission reduction.[30] Combining the above-mentioned analysis with the actual characteristics of thermoelectric flue gas, this paper takes the circulating fluidized bed (CFB) boiler of a power plant with biomass blending as the research object and, with the help of the computational fluid dynamics (CFD) method, the flue gas generated by its biomass blending flue gas. This study was carried out to explore the optimization of the SNCR method to improve the denitrification efficiency while solving the problem of excessive ammonia escape.

2. EXPERIMENTAL SUBJECT AND METHODS

2.1. Experimental Subject. The boiler model is built according to the actual boiler size 1:1, and the views are shown in Figure 1. This boiler adopts the method of biomass blending to control the emissions of pollutants, such as sulfur dioxide and nitrogen oxides, in the combustion process. The design coal type of boiler fuel is raw coal from Huolin River in Inner Mongolia; the calibration coal type is Tiefa Xiaonan mine final coal; the blended biomass is peanut shells, and the results of industrial analysis and elemental analysis of the fuel are shown in Table 2.

From Table 2, it can be found that biomass fuel has the following characteristics compared with coal: (1) higher volatile content, so biomass fuel is easier to ignite and can make the furnace temperature rise faster; (2) higher hydrogen and oxygen content, the H radicals and O radicals generated during combustion can inhibit the formation of NO to a certain extent;

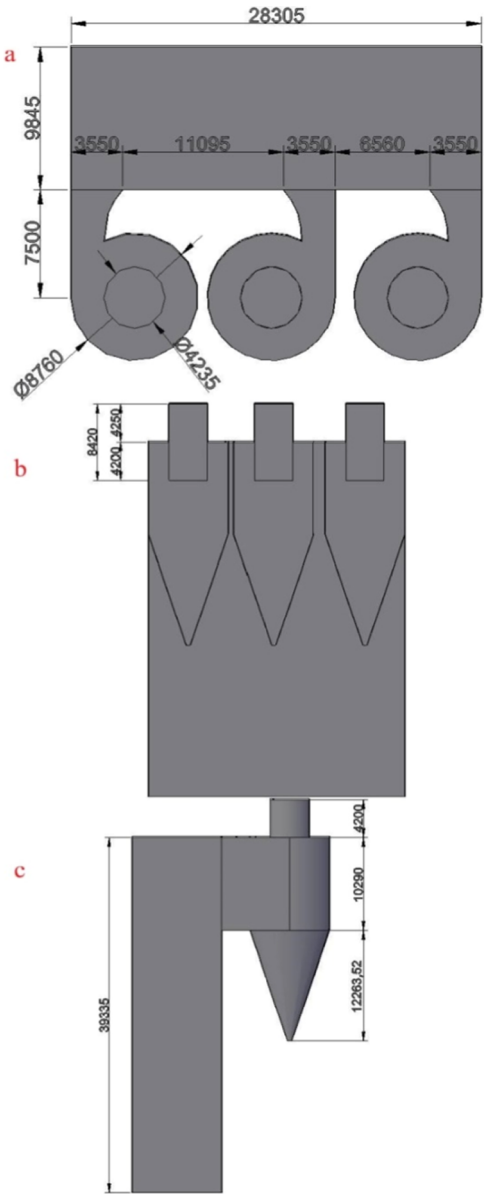

Figure 1. Boiler model structure diagram. (a) top view, (b) cyclone center axis section, and (c) left view.

and (3) lower nitrogen and sulfur content, the content of N and S in biomass is significantly lower than that of coal, the sources of pollutants such as NO_x and SO_2 produced during combustion will be reduced, thus reducing the load of subsequent flue gas pollution control procedures. The biomass fuel selected for this experiment was peanut shells, and most boilers selected wood,[31−34] bark,[32] herbs,[33] cotton stalks,[35] olive waste,[36] and bagasse[34] for blending, and accordingly, there is a certain lack of research on denitrification of flue gas produced by boilers blended with peanut shells. Because common biomass fuels are richer in water and nitrogen contents compared to coal[37] and the peanut shell biomass fuel selected for this study has lower water and nitrogen contents than the coal used, the flue gas produced by its blending differs from other cases, so this paper is a targeted study of flue gas denitrification treatment with less water vapor.

The NO_x control method used in this research subject is the SNCR method, with urea as the reducing agent. In addition to the temperature window for optimal reduction, the performance of SNCR technology depends on factors, such as mixing and

https://doi.org/10.1021/acsomega.3c07288
ACS Omega 2024, 9, 10207−10219

Table 2. Industrial and Elemental Analysis of Various Combustibles

	industrial analysis (wt %)			elemental analysis (wt %)				
	M_{ar}	V_{ar}	A_{ar}	C_{ar}	H_{ar}	O_{ar}	N_{ar}	S_{ar}
design coal type	28.10	25.19	20.91	37.46	2.95	9.47	0.64	0.47
check coal type	8.30	19.74	43.08	38.41	2.86	6.49	0.54	0.32
biomass	18.24	58.12	7.28	17.88	4.57	35.82	0.44	0.07

Table 3. SNCR Reaction Mechanism with Urea as a Reductant[a]

reaction	A (mol·s^{-1})	b	E (J·mol^{-1})
$CO(NH_2)_2 \rightarrow NH_3 + HNCO$ (1)	1.27×10^4	0	65048.109
$CO(NH_2)_2 + H_2O \rightarrow 2NH_3 + CO_2$ (2)	6.13×10^4	0	87819.133
$NH_3 + NO \rightarrow N_2 + H_2O + H$ (3)	4.24×10^2	5.30	349937.06
$NH_3 + O_2 \rightarrow NO + H_2O + H$ (4)	3.50×10^{-1}	7.65	524487.005
$HCNO + M \rightarrow H + NCO + M$ (5)	2.40×10^8	0.85	284637.8
$NCO + NO \rightarrow N_2O + CO$ (6)	1.00×10^7	0	−1632.4815
$NCO + OH \rightarrow NO + CO + H$ (7)	1.00×10^7	0	0
$N_2O + OH \rightarrow N_2 + O_2 + H$ (8)	2.00×10^6	0	41858.5
$N_2O + M \rightarrow N_2 + O + M$ (9)	6.9×10^{17}	−2.5	271075.646

[a]A is the prefinger factor; b is the temperature index; E is the reaction activation energy; and M is an unknown inert component, which is not involved in the simplified kinetic mechanism.

residence time. During the design process, it is necessary to consider not only the accurate representation of all factors but also the analysis of the nonlinear combinations between them, which require a comprehensive analysis of turbulent hydrodynamics, radiation, convective heat transfer, spray droplet dynamics, and gas-phase chemistry in advance,[38] which can be achieved with a reasonable numerical simulation using a CFD code that includes SNCR chemistry. As early as 1990, Nalco Fuel Technologies (NFT) in the United States, in collaboration with Michels et al., used CFD simulations to guide the design and optimization of full-scale SNCR systems.[39] Han et al. developed a skeleton mechanism with 105 reactions based on the detailed mechanism "GADM98" and a subsequent 10-step simplified mechanism for mixed reignition/SNCR of methane and ammonia and implemented it into a 3D combustion CFD program to simulate the complex reignition/SNCR process, and both the simplified mechanism and the integrated model gave satisfactory results over a wide range of parameters.[40] Model simulations were in reasonable agreement with the experimental data and were more similar to those of the detailed kinetic model above 900 °C.[41] Nguyen et al. also reported in 2010 that the combined SNCR-SCR simulation test they did was the same as the pilot experiment, with the lowest NO concentration at 940 °C, but the experimental data differed from the simulated data by 13% at 980 °C.[42] Lv et al. developed a simplified mechanism for an SNCR system with urea as the reducing agent, and its applicability was rigorously verified under a wide range of operating conditions, with concentration errors of almost all important substances below 10% except for N_2O in the high-temperature region.[43] Xia et al. proposed a CFD scheme to simulate the injection location, injection rate, and nonstandard stoichiometry ratio (NSR) for a 750 t/d commercial incinerator with a three-dimensional critical point velocity and nonstandard stoichiometric ratio (NSR) on SNCR performance, and the results showed that the highly heterogeneous distribution of gas velocity, temperature, and NO_x concentration made the injection location one of the most sensitive operating parameters affecting SNCR performance of a moving-grate incinerator.[44] For SNCR applications in industrial boilers with limited space, to improve the NO reduction efficiency, Shin et al. developed a comprehensive computer program, and according to the calculations, NO can be removed more efficiently due to the increase in injection rate and the increase in the depth of penetration of the reductant.[45] Liu and Kao simulated the predecomposer combustion and urea aqueous solution-based SNCR process by CFD and investigated different injection flow rates and stratified injection at different flow rates in the SNCR process, and the results showed that different injection heights and different injection flow rates have a significant effect on NO_x removal efficiency and NH_3 leakage.[46]

2.2. Experimental Methods. Computational fluid dynamics is the simulation and analysis of hydrodynamic problems by solving the controlling equations of fluid dynamics by computer and numerical methods. The use of CFD requires first extraordinary computational power and time and second improvements in realistic turbulence models, turbulence−chemical interactions, and available simplified reaction mechanisms to improve accuracy and applicability. Also, modeling of real equipment with full chemical properties and delineating a fine enough mesh is required to obtain reasonable simulation results.[47]

2.2.1. Reaction Mechanism. As a basis for CFD simulations, there are three accurate, rational, controllable, generic, and portable SNCR denitrification reaction mechanisms, which are the thermal $DeNO_x$ mechanism with NH_3 as the reducing agent,[48] the NO_xOUT mechanism with urea as the reducing agent,[49] and the $RAPRENO_x$ mechanism with cyanuric acid as the reducing agent.[50] In this study, numerical simulations were carried out using ANSYS 2021 R1 software, using the SNCR calculation module in which the reaction mechanism consists of a two-step urea decomposition mechanism and a seven-step reduction kinetic mechanism, as detailed in Table 3.

2.2.2. Model Building. In the CFD method, model building is a very important step, which should be close to reality to reduce

https://doi.org/10.1021/acsomega.3c07288
ACS Omega 2024, 9, 10207−10219

the deviation of the results but also to simplify as much as possible to reduce the computational load. Therefore, the following ideal conditions for simplification are set: (1) calculate only the single-phase steady-state flow field in the reaction zone, without considering the perturbation of the reaction by particles; (2) assume that the main components of the flue gas are N_2, O_2, CO_2, NO, and water, the specific shares are given by the data provided by the docked companies, and that the components of the flue gas and the reductant gas are incompressible ideal gases; (3) the flue wall is set as a smooth heat transfer wall, and the evaporation process of liquid droplets is set by the DPM model; and (4) ignore some internal structures that have less influence on the flow field, such as the frame and beam in the system.

The MESH module in WorkBench is used to mesh the model, and the cyclone part, which mainly generates the reaction, is divided into a tetrahedral mesh and encrypted and named cyclones 1, 2, and 3 along the positive direction of the *Y*-axis.

To eliminate the influence of meshing on the calculation results, the grid independence verification is carried out, and the model is divided into 112,447, 239,849, and 323,739 grids; the simulation results show that the mass flow difference between import and export is 9.60, 3.24, and 0.24 mg/s, respectively. The greater the number of grids, the smaller the error of the calculation results but the slower the calculation speed. The rougher the grid, the greater the error of the calculation results but the calculation speed is faster. Taking into account the calculation accuracy and speed, the model is finally divided into 239,849 grids as shown in Figure 2.

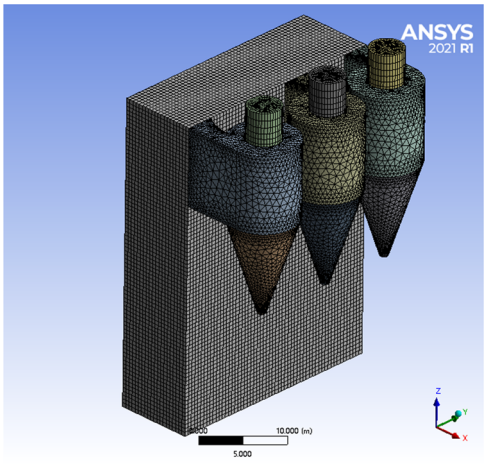

Figure 2. Mesh division diagram.

2.2.3. Physical Model Selection. When setting up the numerical simulation solver, it is necessary to select the appropriate physical models according to the calculated problem, including the multiphase flow model, energy equation, turbulence model, radiation model, component transport and reaction model, discrete phase model, solidification and melting model, and aerodynamic noise model. In this study, we need to open the energy equation to simulate the heat transfer process such as droplet evaporation, choose the standard k-ε model for the turbulence model to simulate the gas flow, open the component transport and reaction model to simulate the interaction between the fluid and reductant, and open the discrete phase model to simulate the injection of the reductant.

2.2.4. Boundary Condition Setting. The boundary conditions are the mathematical physical conditions that the flow field variables should satisfy at the computational boundary. The boundary conditions together with the initial conditions are called fixed solution conditions, and the solution of the flow field exists and is unique only after the boundary conditions and initial conditions are determined. The initial conditions of Fluent are performed during the initialization process, while the boundary conditions need to be set separately. The boundary conditions are roughly divided into fluid inlet and outlet conditions, wall conditions, internal cell partitioning, and internal surface boundary conditions. The inlet flue gas flow rate is 279 m^3/s, divided by the inlet area, and the inlet velocity is about 1 m/s, so the inlet in this model is set as a velocity inlet with a velocity size of 1 m/s, turbulence intensity of 10%, hydraulic diameter of 14.56 m, and temperature of 1200 K, the mass fraction of each component is shown in Table 4, and the outlet is a pressure outlet with a gauge pressure of 0. The rest of the conditions are kept as default.

Table 4. Imported Flue Gas Composition

components	O_2	H_2O	CO_2	NH_3	NO
mass fraction (%)	2	11.6	16.3	0.02	0.05

Under this boundary condition, no injection source was set, and the model was initialized and iteratively calculated in 1500 steps to obtain the NO distribution maps of the entire fluid domain, the three outlets, and the central axis profile of the cyclone (Figure 3), and the area-weighted average NO concentrations of the resulting output for each face are filled in Table 5. At this time, the NO concentration is close to the actual NO_x distribution in the boiler when SNCR measures are not added, the NO velocity at the inlet is 134 mg/s when converted, the difference in NO concentration distribution in the three cyclones is negligible, a reductant injection source is proposed to be set up in each cyclone, and the flow rate of the three injection sources is consistent.

3. RESULTS AND DISCUSSION

Once the burner starts to operate, the internal flow field is inevitably disturbed, resulting in static values that are not applicable. The only way to reduce the NO_x emissions is to overinject the reductant, which leads to two problems: the overinjection of the reductant on the reactor wall will cause costumes and the incomplete reaction of NH_3 will cause ammonia to escape beyond the guaranteed value. To address the above-mentioned problems, numerical simulations were used to optimize the SNCR system by adjusting the injection flow rate, injection speed, nozzle distribution, and other relevant parameters, taking into account the current experimental test conditions.

3.1. Injection Volume Optimization. The mixed combustion of biomass with a low nitrogen content reduces the nitrogen content of the same quality fuel, thus reducing the formation of fuel-type NO_x to a certain extent. At the same time, due to the low water content of biomass and the decrease of the levels of OH and O in the flue gas during combustion, the conversion of NH_i and N_2 to NO_x was inhibited. To sum up, the mixed burning of biomass with a low nitrogen content and low water content can effectively reduce the formation of NO_x in the flue gas, and the NO_x in the boiler is about 130 mg/m^3. The normalized stoichiometric ratio (NSR) was obtained from the

https://doi.org/10.1021/acsomega.3c07288
ACS Omega 2024, 9, 10207−10219

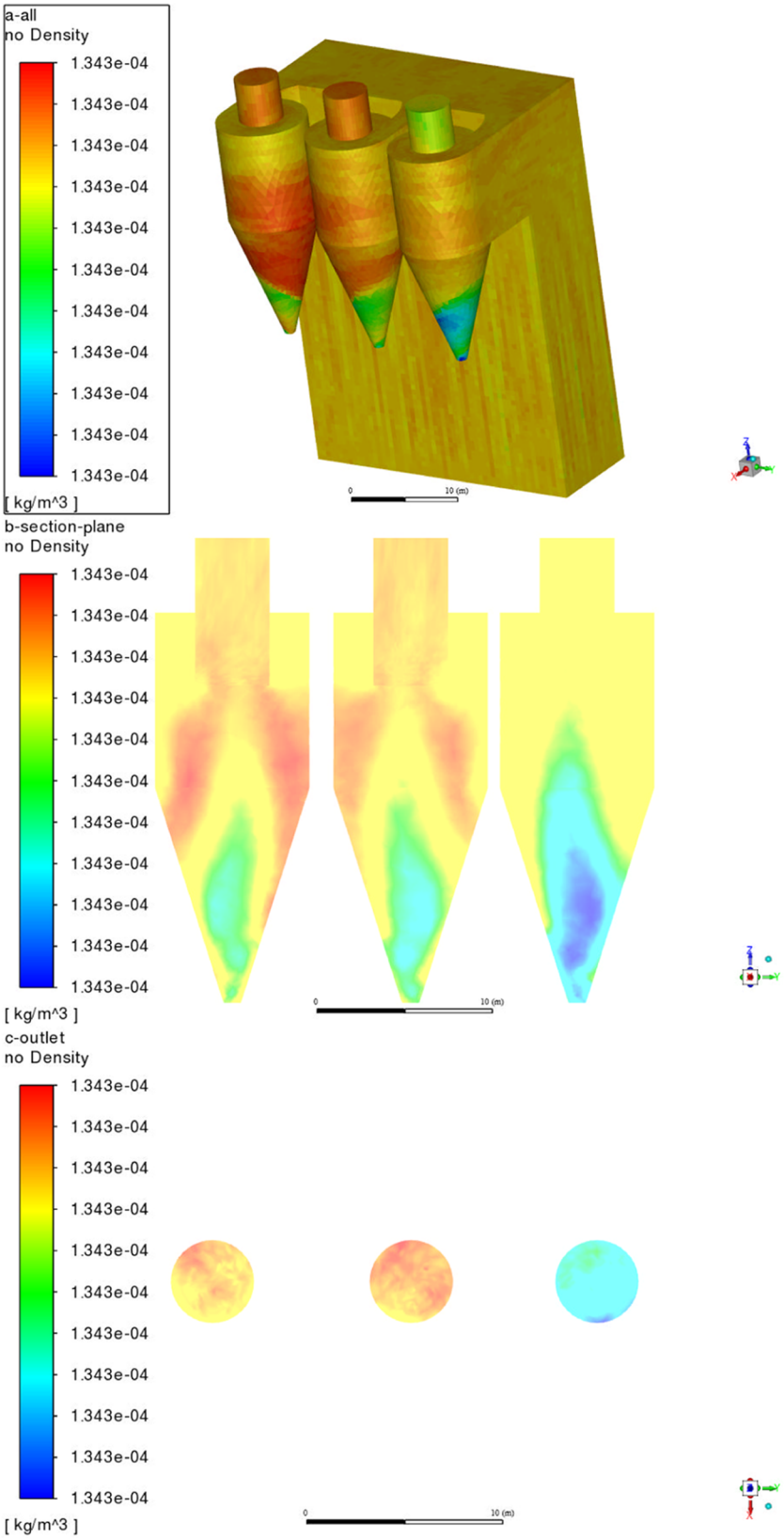

Figure 3. NO concentration distribution without injection of a reducing agent.

Table 5. Area-Weighted Average of NO Density from Surfaces

surfaces	inlet	outlet-1	outlet-2	outlet-3	section plane
area-weighted average of NO density (mg/m^3)	134.264	134.266	134.266	134.264	134.264

https://doi.org/10.1021/acsomega.3c07288
ACS Omega 2024, 9, 10207−10219

actual molar ratio of urea to initial NO over the stoichiometric molar ratio of urea to initial NO. The urea solution with a mass concentration of 10% was selected as the reducing agent, and the total flow rate of the reducing agent should be 0.0374 kg/s and NSR = 1. Numerous studies have shown that the NSR between 0.5 and 2 is more appropriate,[44,51,52] and the denitrification efficiency is lower for too small an ammonia-to-nitrogen ratio, and the ammonia escape rate increases significantly for too large an ammonia-to-nitrogen ratio. Therefore, in this experiment, the NSR was selected as 0.5, 0.75, 1, 1.25, 1.5, 1.75, and 2 gradient flow rates of reductant injection to investigate the effect of injection volume on reduction efficiency and ammonia escape. One injection source was set at the top of each cyclone inlet pipe, set to a conical shape, and the parameters of the injection source are shown in Table 6. The injection speed of the injection source was 1 m/s, and the simulation results at different flow rates were obtained, as shown in Figure 4.

Table 6. Properties of Injections

property	value		
number	1	2	3
X-position (m)	2.227	2.227	2.227
Y-position (m)	1.05	17.144	27.255
Z-position (m)	0	0	0
diameter (m)	0.0001	0.0001	0.0001
temperature (K)	300	300	300
X-axis	0	0	0
Y-axis	0	0	0
Z-axis	−1	−1	−1
velocity magnitude (m/s)	50	50	50
cone angle (deg)	30	30	30
radius (m)	0	0	0

As can be seen from Figure 4, the NO concentration at the outlet decreases significantly with the increase of the NSR, and after reaching 1.25, the decreasing trend of the NO concentration slows down and even increases slightly. On the other hand, the concentration of NH_3 at the outlet increases sharply as NSR increases from 0.5 to 1.25, and then, the increasing trend slows down. This indicates that for a NSR less than 1.25, the denitrification efficiency is positively correlated with the ammonia-to-nitrogen ratio and the NO reduction reaction dominates and is accompanied by a large amount of NH_3 consumption. After NSR > 1.25, the NO reduction efficiency has reached its limit, and the growth rate of NH_3 decomposed by the urea solution begins to exceed the NH_3 consumption rate of reduced NO so that more NH_3 passes through the R4 reaction to generate part of the NO, leading to a paradoxical increase in the outlet NO concentration. Therefore, the optimal ammonia-to-nitrogen ratio should be taken as NSR = 1.25, when there are high denitrification efficiencies of 81.00, 81.63, and 82.74% at the three outlets, and ammonia escapes of 1.76, 2.08, and 9.42 mg/s are within a reasonable range. The comparison of the velocity flow field inside the model for a single injection source flow rate of 0 versus 0.25 kg/s is shown in Figure 5.

3.2. Optimization of the Number of Injection Sources.

From the comparison in Figure 5, it can be seen that due to the influence of the injection source on the flow field, the flow line near the cyclone inlet and inside becomes uneven, and there is a more obvious difference in the amount of ammonia fugitive. In order to improve this phenomenon, an injection source is added to the side of each cyclone inlet channel away from the center line, numbered 4, 5, and 6, and the cone angle is set to 60°; the position parameters of these three injection sources are shown in Table 7.

By increasing the number of injection sources and thus reducing the individual injection source flow rates, the ultimate goal is to reduce the effect of the reductant droplet bundle on the flow field.The uniformly distributed flow rates of injection sources 1−6 are 0.05 kg/s, and the injection flow rates are all 1 m/s. The turbulence−chemistry interaction of the component transport model is changed from the eddy dissipation concept to

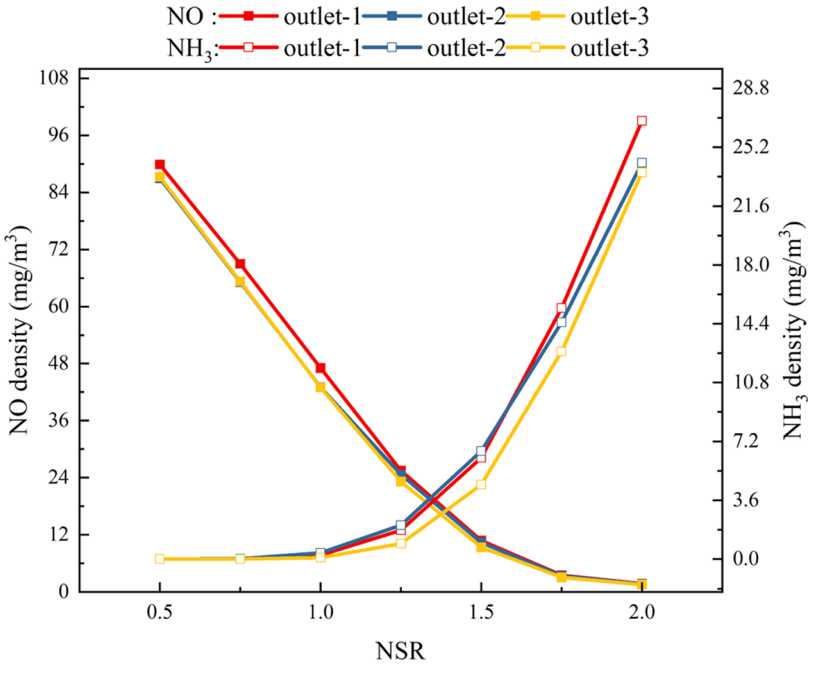

Figure 4. Change of NO and NH_3 at the outlets with the NSR.

https://doi.org/10.1021/acsomega.3c07288
ACS Omega 2024, 9, 10207−10219

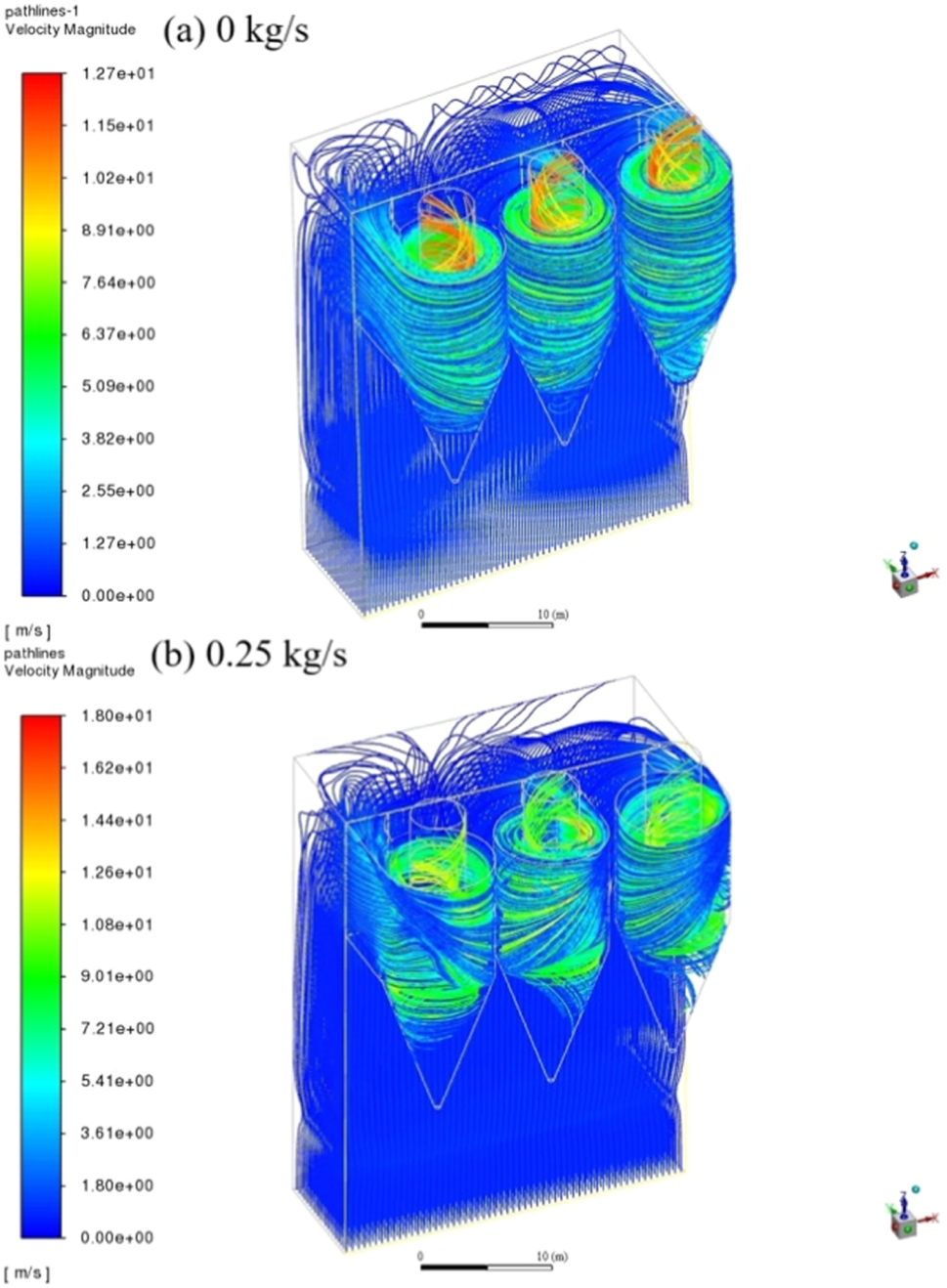

Figure 5. Velocity flow field inside the model when the flow rates of the injection source are 0 and 0.25 kg/s.

Table 7. Side Single Injection Source Position and Injection Direction Parameters

property	value		
number	4	5	6
X-position (m)	2.227	2.227	2.227
Y-position (m)	0	18.195	28.305
Z-position (m)	−5	−5	−5
X-axis	0	0	0
Y-axis	1	−1	−1
Z-axis	0	0	0

Finite-Rate/No TCI, only the turbulent interaction between discrete and continuous phases is examined, and the detailed chemical reaction mechanism of NH_3 and NO is no longer calculated to reduce the computational load. The distribution of the turbulent intensity k of the cylindrical cross-section at the cyclone inlet was used to determine the degree of influence of the injection source on the turbulence of the flow field, and the simulation results were obtained as shown in Figure 6, and the area-weighted uniformities K_1, K_2, and K_3 of the three cross-sections k are compared in Table 8.

From the comparison of Figure 6a,b, it can be seen that the increase of the injection source causes a significant reduction of the NH_3 concentration gradient at the inlet and central cylinder part, which indicates that the mixing of NH_3 and the flue gas is better at this time, and the tendency of diffusion to the lower part of the cyclone is more significant, and the reducing agent has a longer residence time. Figure 6c,d shows that after increasing the number of injection sources, the extreme difference in turbulence intensity at the inlet of each cyclone is reduced, the

https://doi.org/10.1021/acsomega.3c07288
ACS Omega 2024, 9, 10207−10219

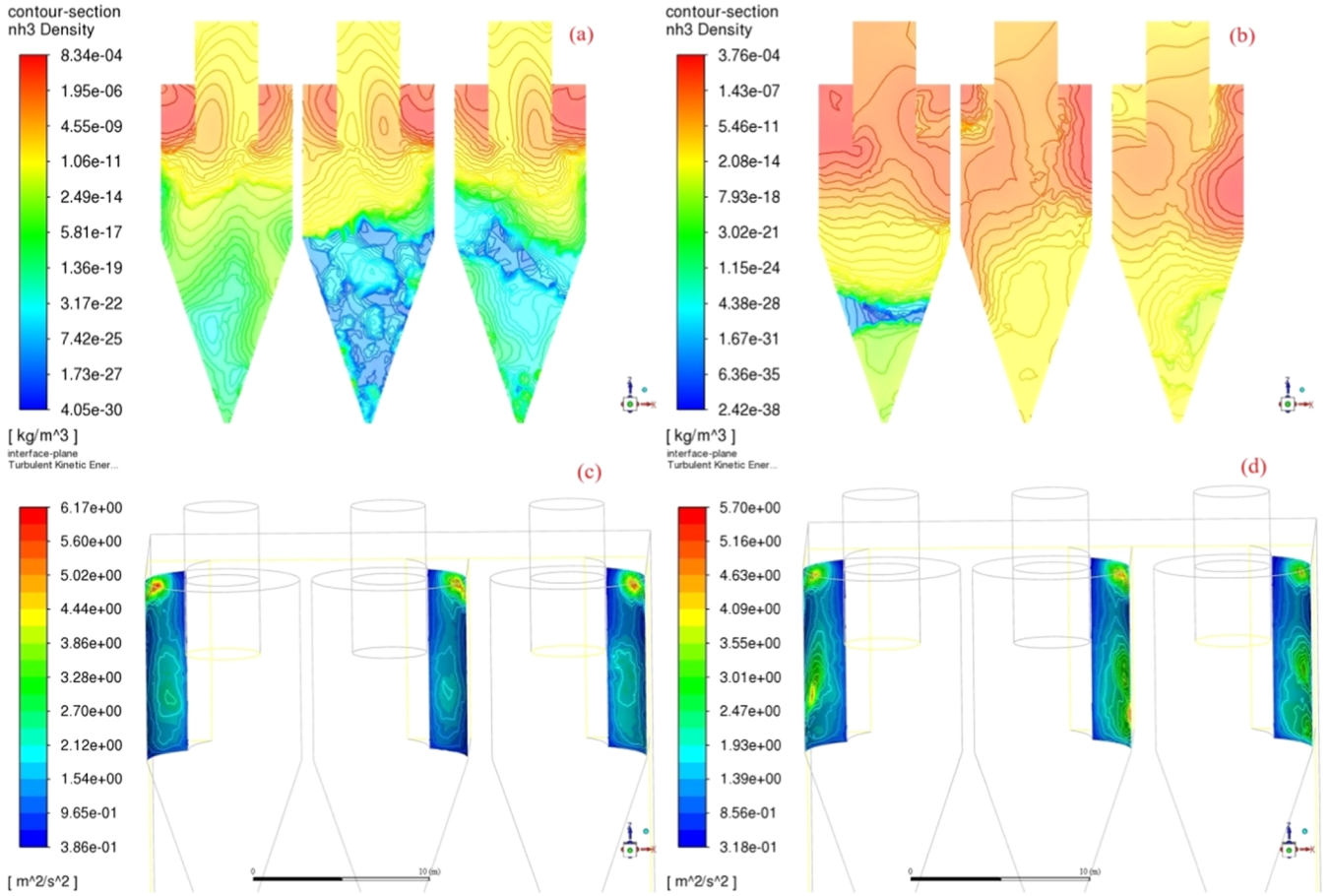

Figure 6. Simulation results when the flow rate of six injections is 0.05 kg/s and the injection velocity is 1 m/s.

Table 8. Area-Weighted Uniformity of Turbulence Intensity of the Cyclone Inlet Section under Different Numbers of Injections

area-weighted uniformity (%)	K_1	K_2	K_3
3 injection × 0.1 kg/s	83.153617	82.056921	81.909084
6 injection × 0.05 kg/s	84.00257	85.533178	82.845563

peak values of k at the upper and lower parts are more similar, and the distribution of turbulence intensity is more reasonable, which can also be seen from the values in Table 8, and it is this that results in a more uniform distribution of NH_3. On the one hand, due to the reduction of the injection volume, the kinetic energy carried by the reductant droplets at the same speed is reduced, so the flow field of the flue gas is less perturbed; on the other hand, the two injection sources in the same inlet channel affect each other, the injection velocity direction is orthogonal,

Table 9. Injection Source Position and Injection Direction of Four Schemes

schemes	coordinates and injection direction	injection-1	injection-2	injection-3	injection-4	injection-5	injection-6
1	*X* coordinate (m)	2.227	2.227	2.227	2.227	2.227	2.227
	Y coordinate (m)	1.05	0	17.144	18.105	27.255	28.305
	Z coordinate (m)	0	−5	0	−5	0	−5
	injection direction	−*Z*	*Y*	−*Z*	−*Y*	−*Z*	−*Y*
2	*X* coordinate (m)	2.227	2.227	2.227	2.227	2.227	2.227
	Y coordinate (m)	1.05	1.05	17.144	17.144	27.255	27.255
	Z coordinate (m)	−2	−8	−2	−8	−2	−8
	injection direction	−*X*	−*X*	−*X*	−*X*	−*X*	−*X*
3	*X* coordinate (m)	0	0	0	0	0	0
	Y coordinate (m)	1.05	1.05	17.144	17.144	27.255	27.255
	Z coordinate (m)	−2	−8	−2	−8	−2	−8
	injection direction	−*X*	−*X*	−*X*	−*X*	−*X*	−*X*
4	*X* coordinate (m)	0	2.227	0	2.227	0	2.227
	Y coordinate (m)	1.05	1.05	17.144	17.144	27.255	27.255
	Z coordinate (m)	−5	−5	−5	−5	−5	−5
	injection direction	−*X*	−*X*	−*X*	−*X*	−*X*	−*X*

https://doi.org/10.1021/acsomega.3c07288
ACS Omega 2024, 9, 10207−10219

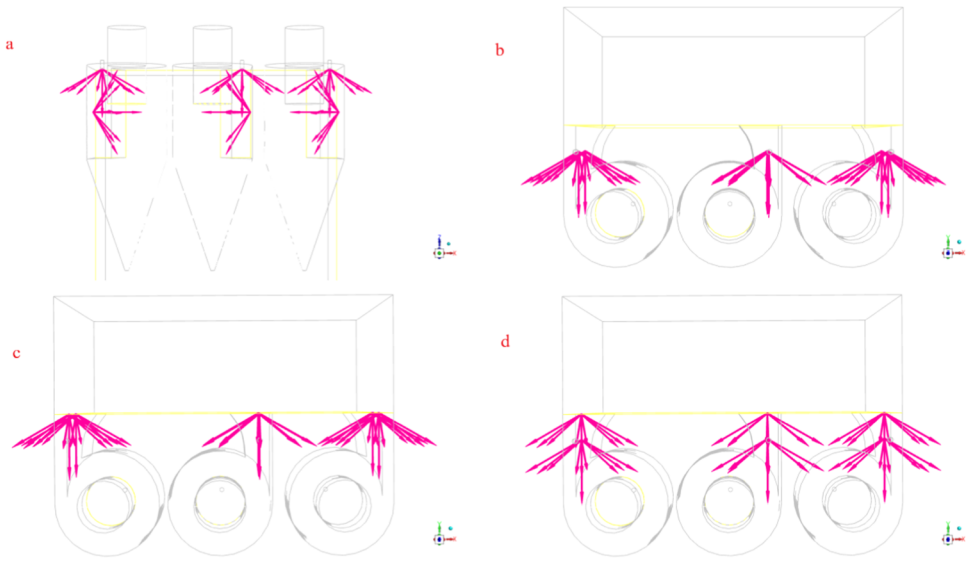

Figure 7. Four distribution schemes of injection source. (a) Scheme 1, (b) Scheme 2, (c) Scheme 3, and (d) Scheme 4.

and the collision of the two clusters of the reductant droplet flow cancels part of the kinetic energy, thus reducing the perturbation of the flue gas flow field.

3.3. Optimization of the Relative Positions of the Injection Sources. Considering that the flow field is greatly influenced by the injection source, it is possible that the jet direction of the injection source is orthogonal to the flue gas flow direction, which has a large disturbance. Therefore, we try to change the injection direction and the relative position of the injection source to reduce the disturbance and improve the mixing uniformity of the reducing agent and flue gas. Four distribution schemes were set up, and the area-weighted uniformity index of NH_3 at the inlet of the central cylinder was used as the evaluation criterion for the homogeneity of the reductant mixture. The parameters of the four distribution scheme positions are shown in Table 9, and each separator is set up with two injection sources, six in total, with a jet angle of 60°, a flow rate of 50 m/s, and a flow rate of 0.24 kg/s. The rest of the parameters are the same as before, and the specific distribution positions are shown in Figure 7.

In order to avoid the reaction of NH_3 from urea decomposition with other gas components in the model, which affects the accuracy of the simulation, it is necessary to turn off the NO_x generation model and modify the inlet boundary conditions so that the incoming gas is only N_2 that will not react with the reductant, which will also reduce the computational load and make the iterative calculation converge faster. The four distribution schemes are set up separately, and the area mass integral uniformity index of NH_3 at the inlet of the central cylinder is used as the evaluation criterion for the uniformity of the reductant mixture. Among them, the scheme 1 arrangement is similar to Sections 3.1 and 3.2 as the control group, the remaining three injection directions are parallel to the flue gas velocity direction as the experimental group, and the simulation results of the four groups are shown in Table 10.

From the above-mentioned table, it can be seen that the uniformity of the NH_3 distribution obtained by the rest of the injection source arrangement is improved to some extent compared to Scheme 1. This proves that the mixing effect of the reductant and flue gas is stronger when the injection direction is the same as the flue gas flow direction than when they are

Table 10. NH_3 Uniformity of Center Cylinders under Different Injection Source Distributions

NH_3 distribution uniformity (%)	Scheme 1	Scheme 2	Scheme 3	Scheme 4
left-center cylinder	91.1	96.1	99.4	94.2
intermediate-center cylinder	92.8	94.4	98.5	94.5
right-center cylinder	88.1	96.4	93.4	98.7

orthogonal. The slightly lower uniformity of Scheme 4 compared to Schemes 2 and 3 is due to the fact that the two injection sources in the inlet pipe of the same cyclone are on the same *Y*-axis, and the injection cone angles are overlapping on the orthogonal projection of the flue gas velocity, so that at the same diffusion velocity, the reductant injected by the two injection sources located on different *Y*-axes has a larger distribution range in the *Z*-direction, resulting in a higher uniformity.

3.4. Optimizing Applications. Based on the above-mentioned analysis, the optimal spray source layout is selected as NSR = 1.25, with each of the six spray sources having a flow rate of 0.078125 kg/s, and the location distribution is Scheme 3. The data obtained from numerical simulation and practical boiler applications are listed in Table 11.

During the actual operation of the boiler, there will be fluctuations in the flue gas flow rate, temperature, oxygen content, and nitrogen oxide concentration within a certain range, which can affect the mixing effect of the reducing agent, resulting in differences between the simulation results and the actual results. On the other hand, during the actual operation,

Table 11. Comparison between Numerical Simulation and Actual Boiler Data

project	numerical simulation	practical boiler applications
temperature (K)	1200	1221.15
O_2 volume fraction (%)	4.065	2.4
NO_x concentration (mg/m^3)	134.3	128.5
NSR	1.25	1.25
denitration efficiency (%)	83.4	74.2
ammonia escape (mg/m^3)	1.1	2.7

https://doi.org/10.1021/acsomega.3c07288
ACS Omega 2024, 9, 10207−10219

the gas composition generated by the boiler is complex, and there may also be oxidizing substances in the circulating ash unique to the circulating fluidized bed, which lead to additional consumption of reducing agents. This also leads to a lower actual decommissioning efficiency than the simulation results. However, overall, after optimization design, the boiler denitrification efficiency has been significantly improved, and the nitrogen oxide emissions and ammonia escape meet ultralow emission standards.

4. CONCLUSIONS

(1) In the numerical simulation of flue gas SNCR method denitrification using Fluent, the injection volume can be optimized according to the NO and NH_3 distribution clouds in the simulation results. Therefore, in this experiment, the reductant injection with an NSR of 0.5, 0.75, 1, 1.25, 1.5, 1.75, and 2 gradient flow rates was selected to investigate the effect of injection volume on reduction efficiency and ammonia escape. Before the NSR increased to 1.25, NO reduction efficiency and NH3 increased with the increase of the reductant, and after NSR > 1.25, the effect of the continued increase of the reductant on denitrification efficiency and ammonia escape rate was no longer obvious, so the optimized ammonia-to-nitrogen ratio was set to NSR = 1.25.

(2) Appropriate adjustment of the number of injection sources can improve the flue gas flow field. When the amount of the reductant required for the SNCR reaction is too large, too few injection sources and too large injection volume will produce more obvious disturbance to the flue gas flow field; at this time, the number of injection sources can be appropriately increased and the flow rate of each injection source can be apportioned to reduce its disturbance to the flow field.

(3) Changing the direction of injection and the distribution of injection sources can be appropriate to enhance the uniformity of the reductant mixture. Changing the direction of injection from perpendicular to the flue gas velocity to parallel and the line of injection sources at a certain angle to the direction of the flue gas velocity, both help the diffusion of the reducing agent.

(4) Selecting NSR = 1.25 and arranging the injection source as Scheme 3, the boiler was retrofitted to achieve an actual denitrification efficiency of 74.2% and an ammonia escape rate of 2.7 mg/m^3, meeting the ultralow emission requirements.

AUTHOR INFORMATION

Corresponding Author

Yu Gao − *School of Environment and Chemical Engineering, Shenyang University of Technology, Shenyang, Liaoning 100870, China;* orcid.org/0009-0006-6733-1439; Email: gaoyu1000@163.com

Authors

Linmao Pu − *School of Environment and Chemical Engineering, Shenyang University of Technology, Shenyang, Liaoning 100870, China;* orcid.org/0009-0003-8000-1272

Shengjun Zhong − *School of Metallurgy, Northeastern University, Shenyang, Liaoning 110819, China*

Yong Zhang − *Atmospheric Administration, Shenyang Ecological Environment Monitoring Center of Liaoning Province, Shenyang, Liaoning 110161, China*

Penglei Zhao − *Ecological Environment Assessment Room, Ecological Environmental Protection Science and Technology Centre of Liaoning Province, Shenyang, Liaoning 100161, China*

Lijuan Ji − *School of Environment and Chemical Engineering, Shenyang University of Technology, Shenyang, Liaoning 100870, China;* orcid.org/0009-0008-0564-6691

Xinyu Liu − *School of Environment and Chemical Engineering, Shenyang University of Technology, Shenyang, Liaoning 100870, China*

Zhonghao Yan − *School of Environment and Chemical Engineering, Shenyang University of Technology, Shenyang, Liaoning 100870, China*

Complete contact information is available at: https://pubs.acs.org/10.1021/acsomega.3c07288

Notes

The authors declare no competing financial interest.

ACKNOWLEDGMENTS

The authors would like to express their grateful acknowledgment to the 2020 Liaoning Province "double first-class" construction project (scientific research category) (FWDFGD2020041) and the 2019 Liaoning Provincial Natural Science Foundation Grant Program (2019-MS-202)for their financial support.

REFERENCES

(1) Wang, Z.; Zhou, J.; Zhu, Y.; et al. Simultaneous removal of NOx, SO2 and Hg in nitrogen flow in a narrow reactor by ozone injection: Experimental results. *Fuel Process. Technol.* **2007**, *88*, 817−823, DOI: 10.1016/j.fuproc.2007.04.001.

(2) Gómez-García, M. A.; Pitchon, V.; Kiennemann, A. Pollution by nitrogen oxides: an approach to NOx abatement by using sorbing catalytic materials. *Environ. Int.* **2005**, *31*, 445−467.

(3) Rhimi, B.; Padervand, M.; Jouini, H.; et al. Recent progress in NOx photocatalytic removal: Surface/interface engineering and mechanistic understanding. *J. Environ. Chem. Eng.* **2022**, *10*, No. 108566, DOI: 10.1016/j.jece.2022.108566.

(4) Islam, A.; Teo, S. H.; Ng, C. H.; et al. Progress in recent sustainable materials for greenhouse gas (NOx and SOx) emission mitigation. *Prog. Mater. Sci.* **2023**, *132*, No. 101033, DOI: 10.1016/j.pmatsci.2022.101033.

(5) Van Caneghem, J.; De Greef, J.; Block, C.; et al. NOx reduction in waste incinerators by selective catalytic reduction (SCR) instead of selective non catalytic reduction (SNCR) compared from a life cycle perspective: a case study. *J. Cleaner Prod.* **2016**, *112*, 4452−4460, DOI: 10.1016/j.jclepro.2015.08.068.

(6) Zheng, W.; Zhang, X.; Zheng, Y.; et al. Oxynitride trap" over N/S co-doped graphene-supported catalysts promoting low temperature NH3-SCR performance: Insight into the structure and mechanisms. *J. Hazard. Mater.* **2022**, *423*, No. 127187, DOI: 10.1016/j.jhazmat.2021.127187.

(7) Yan, X.; Liu, J.; Yang, Y.; et al. A catalytic reaction scheme for NO reduction by CO over Mn-terminated LaMnO3 perovskite: A DFT study. *Fuel Process. Technol.* **2021**, *216*, No. 106798, DOI: 10.1016/j.fuproc.2021.106798.

(8) Hu, Z.; Jiang, E.; Ma, X. Numerical simulation on operating parameters of SNCR process in a municipal solid waste incinerator. *Fuel* **2019**, *245*, 160−173, DOI: 10.1016/j.fuel.2019.02.071.

(9) Świeboda, T.; Krzyżyńska, R.; Bryszewska-Mazurek, A.; et al. Advanced approach to modeling of pulverized coal boilers for SNCR

process optimization - review and recommendations. *Int. J. Thermofluids* **2020**, *7*−*8*, No. 100051, DOI: 10.1016/j.ijft.2020.100051.
(10) Twu, B.-W.; Chu, H.; Chien, T.-W. The absorption kinetics of NO in NaClO2/NaOH solutions. *J. Hazard. Mater.* **2001**, *84*, 241−252, DOI: 10.1016/s0304-3894(01)00215-1.
(11) Guo, R.-T.; Pan, W.-G.; Ren, J.-X.; et al. Absorption of NO from simulated flue gas by using NaClO2/(NH4)2CO3 solutions in a stirred tank reactor. *Korean J. Chem. Eng.* **2013**, *30*, 101−104, DOI: 10.1007/s11814-012-0121-1.
(12) Guo, R.-T.; Gao, X.; Pan, W.-G.; et al. Absorption of NO into NaClO3/NaOH solutions in a stirred tank reactor. *Fuel* **2010**, *89*, 3431−3435, DOI: 10.1016/j.fuel.2010.03.020.
(13) Li, B.; Liu, Y.; Zhao, X.; et al. O3 oxidation excited by yellow phosphorus emulsion coupling with red mud absorption for denitration. *J. Hazard. Mater.* **2021**, *403*, No. 123971, DOI: 10.1016/j.jhazmat.2020.123971.
(14) Du, C.; Yi, H.; Tang, X.; et al. Desulfurization and denitrification experiments in SDA system: A new high-efficient semi-dry process by NaClO2. *Sep. Purif. Technol.* **2020**, *230*, No. 115873, DOI: 10.1016/j.seppur.2019.115873.
(15) Basfar, A. A.; Fageeha, O. I.; Kunnummal, N.; et al. Electron beam flue gas treatment (EBFGT) technology for simultaneous removal of SO2 and NOx from combustion of liquid fuels. *Fuel* **2008**, *87*, 1446−1452, DOI: 10.1016/j.fuel.2007.09.005.
(16) Ghriss, O.; Ben Amor, H.; Jeday, M.-R.; et al. Nitrogen oxides absorption into aqueous nitric acid solutions containing hydrogen peroxide tested using a cables-bundle contactor. *Atmos. Pollut. Res.* **2019**, *10*, 180−186, DOI: 10.1016/j.apr.2018.07.007.
(17) Pawelec, A.; Chmielewski, A. G.; Licki, J.; et al. Pilot plant for electron beam treatment of flue gases from heavy fuel oil fired boiler. *Fuel Process. Technol.* **2016**, *145*, 123−129, DOI: 10.1016/j.fuproc.2016.02.002.
(18) Chmielewski, A. G.; Zwolińska, E.; Licki, J.; et al. A hybrid plasma-chemical system for high-NO x flue gas treatment[J]. *Radiat. Phys. Chem.* **2018**, *144*, 1−7, DOI: 10.1016/j.radphyschem.2017.11.005.
(19) Park, J.-H.; Ahn, J.-W.; Kim, K.-H.; et al. Historic and futuristic review of electron beam technology for the treatment of SO2 and NOx in flue gas. *Chem. Eng. J.* **2019**, *355*, 351−366, DOI: 10.1016/j.cej.2018.08.103.
(20) Tang, N.; Liu, Y.; Wang, H.; et al. Mechanism Study of NO Catalytic Oxidation over MnOx/TiO2 Catalysts. *J. Phys. Chem. C* **2011**, *115*, 8214−8220, DOI: 10.1021/jp200920z.
(21) Ding, J.; Zhong, Q.; Zhang, S.; et al. Simultaneous removal of NOX and SO2 from coal-fired flue gas by catalytic oxidation-removal process with H2O2. *Chem. Eng. J.* **2014**, *243*, 176−182, DOI: 10.1016/j.cej.2013.12.101.
(22) Song, Z.; Wang, B.; Yang, W.; et al. Research on NO and SO2 removal using TiO2-supported iron catalyst with vaporized H2O2 in a catalytic oxidation combined with absorption process. *Environ. Sci. Pollut. Res.* **2020**, *27*, 18329−18344, DOI: 10.1007/s11356-020-08042-6.
(23) Liu, L.; Wang, B.; Yao, X.; et al. Highly efficient MnOx/biochar catalysts obtained by air oxidation for low-temperature NH3-SCR of NO. *Fuel* **2021**, *283*, No. 119336.
(24) van der Maas, P.; Harmsen, L.; Weelink, S.; et al. Denitrification in aqueous FeEDTA solutions. *J. Chem. Technol. Biotechnol.* **2004**, *79*, 835−841, DOI: 10.1002/jctb.1057.
(25) Cubides, D.; Guimerà, X.; Jubany, I.; et al. A review: Biological technologies for nitrogen monoxide abatement. *Chemosphere* **2023**, *311*, No. 137147, DOI: 10.1016/j.chemosphere.2022.137147.
(26) Deng, R.; Huo, P.; Chen, X.; et al. Towards efficient heterotrophic recovery of N2O via Fe(II)EDTA-NO: A modeling study. *Sci. Total Environ.* **2023**, *859*, No. 160285, DOI: 10.1016/j.scitotenv.2022.160285.
(27) Razaviarani, V.; Ruiz-Urigüen, M.; Jaffé, P. R. Denitrification of Nitric Oxide Using Hollow Fiber Membrane Bioreactor; Effect of Nitrate and Nitric Oxide Loadings on the Reactor Performance and Microbiology. *Waste Biomass Valorization* **2018**, *10*, 1989−2000, DOI: 10.1007/s12649-018-0223-z.
(28) Wei, Z. S.; Wang, J. B.; Huang, Z. S.; et al. Removal of nitric oxide from biomass combustion by thermophilic nitrification-aerobic denitrification combined with catalysis in membrane biofilm reactor. *Biomass Bioenergy* **2019**, *126*, 34−40.
(29) Wang, Y.; Li, J.; Huang, S.; et al. Evaluation of NOx removal from flue gas and Fe(II)EDTA regeneration using a novel BTF−ABR integrated system. *J. Hazard. Mater.* **2021**, *415*, No. 125741, DOI: 10.1016/j.jhazmat.2021.125741.
(30) Liu, Q.; Zhong, W.; Yu, A.; et al. Co-firing of coal and biomass under pressurized oxy-fuel combustion mode in a 10 kWth fluidized bed: Nitrogen and sulfur pollutants. *Chem. Eng. J.* **2022**, *450*, No. 138401, DOI: 10.1016/j.cej.2022.138401.
(31) Nussbaumer, T. Primary and Secondary Measures for the Reduction of Nitric Oxide Emissions from Biomass Combustion. *Dev. Thermochem. Biomass Convers.* **1997**, 1447−1461.
(32) Mahmoudi, S.; Baeyens, J.; Seville, J. P. K. NOx formation and selective non-catalytic reduction (SNCR) in a fluidized bed combustor of biomass. *Biomass Bioenergy* **2010**, *34*, 1393−1409, DOI: 10.1016/j.biombioe.2010.04.013.
(33) Zeng, T.; Weller, N.; Pollex, A.; et al. Blended biomass pellets as fuel for small scale combustion appliances: Influence on gaseous and total particulate matter emissions and applicability of fuel indices. *Fuel* **2016**, *184*, 689−700.
(34) Daood, S. S.; Javed, M. T.; Gibbs, B. M.; et al. NOx control in coal combustion by combining biomass co-firing, oxygen enrichment and SNCR. *Fuel* **2013**, *105*, 283−292.
(35) Nimmo, W.; Daood, S. S.; Gibbs, B. M. The effect of O2 enrichment on NOx formation in biomass co-fired pulverised coal combustion. *Fuel* **2010**, *89*, 2945−2952.
(36) Wang, X.; Zhang, J.; Xu, X.; et al. Numerical study of biomass Co-firing under Oxy-MILD mode. *Renewable Energy* **2020**, *146*, 2566−2576, DOI: 10.1016/j.renene.2019.08.108.
(37) Dakić, D. V.; Nemoda, S. Đ.; Paprika, M. J.; Komatina, M. S.; Repić, B. S.; Erić1, A. M.; Mladenović, M. R. The combustion of biomass − The impact of its types and combustion technologies on the emission of nitrogen oxide. *Chem. Ind.* **2016**, *70* (3), 287−298, DOI: 10.2298/HEMIND150409033M.
(38) Cremer, M. A.; Montgomery, C. J.; Wang, D. H.; et al. Development and implementation of reduced chemistry for computional fluid dynamics modeling of selective non-catalytic reduction. *Proc. Combust. Inst.* **2000**, *28*, 2427−2434, DOI: 10.1016/S0082-0784(00)80656-6.
(39) Michels, W. F.; Gnaedig, G.; Comparato, J. R. In *The Applications of Computational Fluid Dynamics in NOxOUT Process for Reducing NOx Emissions from Stationary Combustion Sources*, American Flame Research Committee 1990 Fall International Symposium, 1990.
(40) Wei, X.; Schnell, X.; Hein, U.; Han, K. R. G. Detailed modeling of hybrid reburn/SNCR processes for NOX reduction in coal-fired furnaces. *Combust. Flame* **2003**, *132* (3), 374−386.
(41) Nguyen, T. D. B.; Lim, Y.-I.; Kim, S.-J.; et al. Experiment and Computational Fluid Dynamics (CFD) Simulation of Urea-Based Selective Noncatalytic Reduction (SNCR) in a Pilot-Scale Flow Reactor. *Energy Fuels* **2008**, *22* (6), 3864−3876, DOI: 10.1021/ef8004652.
(42) Nguyen, T. D. B.; Lim, Y.-I.; Eom, W.-H.; et al. Experiment and CFD simulation of hybrid SNCR-SCR using urea solution in a pilot-scale reactor. *Comput. Chem. Eng.* **2010**, *34* (10), 1580−1589, DOI: 10.1016/j.compchemeng.2009.12.012.
(43) Lv, Y.; Wang, Z.; Zhou, J.; et al. Development and Validation of a Reduced Mechanism for Urea-based SNCR Process based on QSS Graph. *Energy Fuels* **2009**, *23* (7), 3605−3611, DOI: 10.1021/ef900165k.
(44) Xia, Z.; Li, J.; Wu, T.; et al. CFD simulation of MSW combustion and SNCR in a commercial incinerator. *Waste Manage.* **2014**, *34*, 1609−1618, DOI: 10.1016/j.wasman.2014.04.015.

https://doi.org/10.1021/acsomega.3c07288
ACS Omega 2024, 9, 10207−10219

(45) Shin, M.-S.; Kim, H.-S.; Jang, D.-S. Numerical study on the SNCR application of space-limited industrial boiler. *Appl. Therm. Eng.* **2007**, *27*, 2850−2857, DOI: 10.1016/j.applthermaleng.2006.08.019.
(46) Liu, Y.; Kao, H. Numerical Simulation of Urea Based SNCR Process in a Trinal-Sprayed Precalciner. *J. Renewable Mater.* **2021**, *9* (2), 268−294, DOI: 10.32604/jrm.2021.012015.
(47) Van Hoecke, L.; Boeye, D.; Gonzalez-Quiroga, A.; et al. Experimental methods in chemical engineering: Computational fluid dynamics/finite volume method— CFD/FVM. *Can. J. Chem. Eng.* **2021**, *302*, 545−561, DOI: 10.1002/cjce.24571.
(48) Lyon, R. K. Method for the Reduction of the Concentration of NO in Combustion Effluents Using Ammonia. U.S. Patent US3,900,554, 1975.
(49) Arand, J. K.; Muzio, L. J.; Sotter, J. G. Urea Reduction of NOx in Combustion Effluents. U.S. Patent US4208386A, 1980.
(50) Perry, R. A. No Reduction Using Sublimation of Cyanuric Acid. U.S. Patent US4731231, 1988.
(51) Irfan, N. *Control of Gaseous Emissions by Flue Gas Treatment*; University of Leeds (department of Fuel & Energy), 1995.
(52) Bai, H.; Zhang, Z.; Li, Z.; et al. Industrial Experiment on NO_x Reduction by Urea Solution Injection in the Fuel-Rich Zone of a 330 MW Tangentially Pulverized Coal-Fired Boiler. *Acs Omega* **2022**, *7*, 11853−11861, DOI: 10.1021/acsomega.1c07276.

https://doi.org/10.1021/acsomega.3c07288
ACS Omega 2024, 9, 10207−10219